Available online at www.sciencedirect.com
ScienceDirect
Ceramics International 35 (2009) 1845–1850
CERAMICS INTERNATIONAL
www.elsevier.com/locate/ceramint

Fabrication of submicron alumina ceramics by pulse electric current sintering using M^{2+} (M = Mg, Ca, Ni)-doped alumina nanopowders

Atsushi Odaka, Tomohiro Yamaguchi *, Masahiro Hida, Seiichi Taruta, Kunio Kitajima

Department of Chemistry and Material Engineering, Faculty of Engineering, Shinshu University, 4-17-1 Wakasato, Nagano-shi 380-8553, Japan

Received 8 July 2008; received in revised form 10 September 2008; accepted 7 October 2008
Available online 21 October 2008

Abstract

Dense submicron-grained alumina ceramics were fabricated by pulse electric current sintering (PECS) using M^{2+}(M: Mg, Ca, Ni)-doped alumina nanopowders at 1250 °C under a uniaxial pressure of 80 MPa. The M^{2+}-doped alumina nanopowders (0–0.10 mass%) were prepared through a new sol–gel route using high-purity polyhydroxoaluminum (PHA) and MCl_2 solutions as starting materials. The composite gels obtained were calcined at 900 °C and ground by planetary ball milling. The powders were re-calcined at 900 °C to increase the content of α-alumina particles, which act as seeding for low-temperature densification. Densification and microstructural development depend on the M^{2+} dopant species. Dense alumina ceramics (relative density ≥99.0%) thus obtained had a uniform microstructure composed of fine grains, where the average grain size developed for non-doped, Ni-doped, Mg-doped and Ca-doped samples was 0.67, 0.67, 0.47 and 0.30 μm, respectively, showing that Ca-doping is the most promising method for tailoring of nanocrystalline alumina ceramics.

Keywords: A. Sintering; A. Sol–gel processes; B. Grain size; D. Al_2O_3

1. Introduction

As the grain size of fully dense alumina is reduced, significant benefits are observed in terms of improved mechanical properties [1,2], superior wear resistance [3] and optical transparency [4]. To obtain dense submicron-grained or nanocrystalline alumina ceramics (NCAs), studies on the densification of alumina have focused on the use of nanosized transition alumina powders as a starting powder [5,6]. In these studies, transition aluminas were densified by hot-pressing [5] or sinter-forging [6], and alumina ceramics with an α-alumina grain size of 200 nm or less were obtained. We have also focused on the use of transition alumina powders and attempted densification by pulse electric current sintering (PECS) using polyhydroxoaluminum (PHA) gel-derived γ-alumina powders [7–9]. As a result, we obtained fully densified alumina ceramics with a relatively high bending strength of ∼860 MPa under optimized conditions [9]. However, these alumina ceramics showed an inhomogeneous microstructure consisting of submicron-sized grains and a large number of elongated large grains due to the presence of impurities such as CaO and SiO_2.

It is well known that additives such as MgO [10–13], CaO [14,15] and NiO [11] affect the sintering behavior of α-alumina. MgO plays a particularly beneficial role in inhibiting grain growth of α-alumina, which can be explained in terms of a solute drag (pinning) model [11,12]. While the effect of MO (M: Mg, Ca, Ni) addition to α-alumina powders on grain growth inhibition has been studied extensively, there are few reports concerning the effects of M^{2+}-doping on densification of γ-aluminas except for Mg^{2+}-doping [16]. In particular, systematic studies on the densification behavior induced by PECS for various M^{2+}-doped γ-alumina powders, in which M^{2+} cations are substituted into the crystal lattice of γ-alumina, have been lacking.

Thus, the present study extends the potential applications of the PHA sol–gel process to the intimate mixing of M^{2+} with γ-aluminas through the formation of solid solutions (M^{2+}-doped γ-aluminas) and to the fabrication of high-density submicron-grained alumina ceramics or NCAs by PECS. M^{2+}-doped alumina nanopowders were prepared via a new sol–gel route using high-purity PHA and MCl_2 solutions as starting materials and sintered by PECS. The present study investigated the

* Corresponding author. Tel.: +81 26 269 5417; fax: +81 26 269 5415.
E-mail address: mtmouth@shinshu-u.ac.jp (T. Yamaguchi).

0272-8842/$34.00
doi:10.1016/j.ceramint.2008.10.007

effects of M^{2+}-dopant species on the densification behavior of the M^{2+}-doped alumina nanopowders and the microstructural evolution of the final alumina products obtained by PECS.

2. Experimental

A high-purity PHA solution having an Al_2O_3 concentration of 23.4 mass% and OH/Al ratio of 2.51 was prepared by dissolving Al metal in HCl solution [17,18]. Special attention was paid to the impurities. The sources of divalent cations were $MCl_2{\cdot}nH_2O$ (M = Mg, Ca, and Ni, Wako Pure Chemical Industries). Each chloride was dissolved in distilled water and added to the PHA solution to form 0.10 mass% MO against the mass of Al_2O_3 obtained from the PHA solution, as in the case of Mg^{2+} doping [16]. The mixed solutions were stirred thoroughly at room temperature and then held at 60 °C for 2 days or more for gelation. The resultant composite gels were ground into <150 μm powders using a high-purity alumina mortar and pestle and then calcined at 900 °C for 3 h. The calcined powders were then pulverized by planetary ball milling (LA-$PO_{4/2}$, Ito Works) for 3 h in ethanol using high-purity (99.9%) alumina media. After pulverization, the suspensions were dried and the agglomerates obtained were crushed and sieved through a 140-mesh (<106 μm) screen. The sieved powders were re-calcined at 900 °C for 3 h. The undoped and M^{2+}-doped (M = Mg, Ca, and Ni) alumina nanopowders will hereafter be abbreviated as GA-M0, GA-Mg0.1, GA-Ca0.1 and GA-Ni0.1, respectively. The amounts of impurities (by mass) in GA-Mg0.1, for example, were 44 ppm Si, 4 ppm Na, 7 ppm Ca and 40 ppm Fe, showing that the GA-M-series powders have a high-purity of around 99.99%.

The particle size distribution of GA-M-series powders was measured using a laser diffraction/scattering particle-size analyzer (MT3300, Nikkiso). Their phases before and after pulverization and re-calcination were characterized by XRD. Pore properties such as BET specific surface area and pore volume were measured by N_2 adsorption–desorption isotherms using a specific surface area/pore distribution analyzer (ASAP 2000, Micromeritics). The α-transformation temperatures were determined by DTA.

Each GA-M-series powder (4.0 g) was filled into a graphite mold with an inner diameter of 20 mm and sintered under vacuum by a PECS apparatus (SPS-2050, Sumitomo Coal Mining). PECS was performed at 1250 °C for a holding time of 5 min under a uniaxial pressure of 80 MPa [16]. A heating rate of 200 °C/min was employed with care to prevent overshoot at the sintering temperatures. A carbon paper was inserted in between the graphite punches and graphite mold [19]. The GA-M-series powders were also uniaxially pressed at 300 MPa and sintered by pressureless sintering at 1400 °C in air for comparison. Bulk density of the sintered specimens was measured by the Archimedes method. The raw powders and the microstructure of sintered specimens were observed by a S-3100H scanning electron microscope (SEM) and a JEM 2010 transmission electron microscope (TEM). SEM specimens were mirror polished and thermally etched. TEM samples were prepared by suspending the lightly ground M^{2+}-doped powders in ethanol and evaporating a droplet onto a microgrid. The average grain size of the powders was measured one by one, and the arithmetic average was taken. The average grain size of the sintered samples was estimated by the line-intercept method using at least 150 grain measurements.

3. Results and discussion

3.1. Properties of M^{2+}-doped nanopowders

Fig. 1 shows the XRD patterns of M^{2+}-doped powders calcined at 900 °C for 3 h before planetary ball milling. The undoped powder was γ-alumina with a trace of χ-alumina. The diffraction intensity of χ-alumina, especially its characteristic peak around 42.5° [20], weakened markedly with increasing M^{2+} dopant content and disappeared at 0.5% doping. This implies that M^{2+}-doping is effective in suppressing χ-alumina formation. The diffraction peaks of γ-alumina showed hardly any shift upon 0.1 mass% M^{2+}-doping. However, Mg^{2+} or Ni^{2+}-doped powders having a much higher dopant content (e.g., 15 mass%), which were obtained by calcining at 1000 °C for 3 h, yielded a single-phase γ-alumina with a larger lattice constant than that of the undoped powder obtained under the same calcination conditions [16,21]. This indicates that solid solutions containing M^{2+} cations in the defect spinel lattice of γ-alumina were formed. By contrast, for the Ca^{2+}-doped powders, the increase in the lattice constant saturated around 0.3 mass%, showing that the solubility of Ca^{2+} in the γ-alumina lattice is very low owing to its larger cation size. These results indicate that the dopant cations were substituted even for the Ca series at least up to 0.3 mass%.

XRD patterns of the doped powders after grinding by planetary ball milling were almost identical to those before grinding shown in Fig. 1. This implies that the amount of α-alumina abrasion powders generated by the wear of the pot and

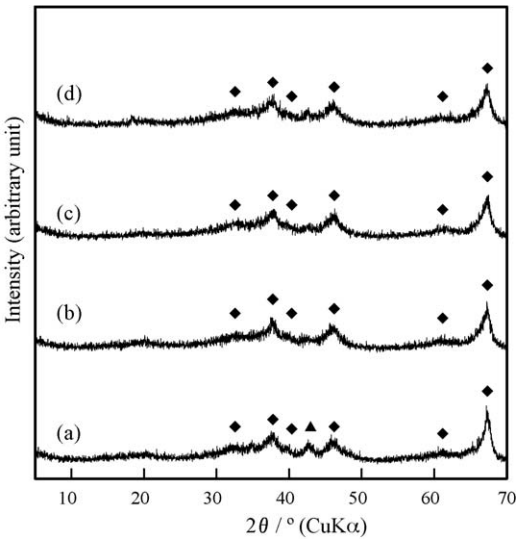

Fig. 1. XRD patterns of M^{2+}-doped powders having different dopants obtained by calcining at 900 °C for 3 h. (a) Undoped, (b) M = Mg, (c) M = Ca and (d) M = Ni. ◆: γ-Al_2O_3, ▲: χ-Al_2O_3.

Table 1
Powder characteristics of the GA-Ms-series samples used for PECS.

Sample	Dopant content (mass%)	Mean particle size of agglomerate (μm)	BET surface area (m^2/g)	α-Fraction (mass%)	Transformation temperature[a] (°C)
GA-M0	0	1.94	36.0	63	943 (1096)
GA-Mg01	0.01	2.01	43.5	48	946 (1121)
GA-Ca01	0.01	2.00	51.7	29	950 (1149)
GA-Ni01	0.01	2.01	48.3	43	948 (1112)

[a] The temperature determined from the onset of the DTA exothermic peak. The temperature of the samples before re-calcination is shown in parentheses for reference.

balls during milling [7] was very small. In the preliminary sintering study, the M^{2+}-doped powders after planetary ball milling for 3 h could not attain full density by PECS at lower sintering temperatures because the seeding effect [7,22] was reduced due to the lower content of α-alumina abrasion powders. Thus, the milled M^{2+}-doped powders were re-calcined at 900 °C for 3 h to enhance the seeding fine α-alumina particles: the re-calcined powders, i.e., GA-M0 and GA-M0.1, were used for the PECS study.

Table 1 summarizes the powder characteristics of GA-Ms used for PECS. The mean particle size of GA-Ms was about 2 μm and corresponded to the size of the agglomerates, which consisted of transition aluminas and α-alumina primary particles. The α-alumina content of the GA-Ms was 63, 48, 29 and 43 mass%, for GA-M0, GA-Mg0.1, GA-Ca0.1 and GA-Ni0.1, respectively. Fig. 2 shows micrographs of GA-Ca0.1 and GA-Ni0.1 powders, indicating that the average particle size of α-alumina was around 100 nm regardless of the dopant species and that these powders consisted of a mixture of α-alumina and γ-alumina nanoparticles. The BET surface area of GA-M0 and GA-M0.1 s ranged from 36.0 to 51.7 m^2/g, corresponding to the variation in the α-alumina fraction of each M^{2+}-doped nanopowder. The pore distribution curve of these powders exhibited a sharp peak around 3.5 nm, which is characteristic of PHA-derived transition alumina [20], and a wide profile around ∼100 nm due to planetary ball milling and α-transformation by re-calcination.

The transformation temperatures (T_p) determined by DTA from the onset of exothermic peaks were 943–950 °C and the α-transformation temperature shifted to slightly higher temperatures with M^{2+}-doping, although the accuracy of the T_p values was very low due to the obscure exothermic profiles. Thus, the T_p of the samples before re-calcination, which is determinable with high accuracy, is also shown in parentheses. The order of the transformation temperatures (T_p) before re-calcination was GA-M0 < GA-Ni0.1 < GA-Mg0.1 < GA-Ca0.1. This coincides with the order reported previously for 0.10 mol% M^{2+}-doped γ-alumina powders [21], despite the different doping base of mol%. The decrease in the transformation temperature by re-calcination can be explained in terms of the increased seeding effect due to the increase in the number of fine α-alumina particles induced by ball milling and re-calcination. The decrease in α-transformation temperature promotes low-temperature densification and the development of a fine-grained microstructure [7,22].

3.2. Densification and microstructural evolution

Fig. 3 shows SEM micrographs of the polished and thermally etched surfaces of sintered GA-M0 and GA-M0.1 samples obtained by PECS at 1250 °C under 80 MPa. The relative density of sintered samples was 99.4%, 99.8%, 99.8% and 98.9%, for GA-M0, GA-Mg0.1, GA-Ni0.1 and GA-Ca0.1, respectively, showing that almost full densification could be attained even for GA-Ca0.1. Sintered GA-M0 (Fig. 3(a)) showed a rather heterogeneous microstructure containing some larger grains (∼1.5 μm). Sintered GA-Mg0.1 (Fig. 3(b)) was pore-free and showed a fine and uniform microstructure consisting of small and equiaxed grains. Sintered GA-Ca0.1 (Fig. 3(c)) showed the finest and most uniform microstructure consisting of smaller and more equiaxed grains. By contrast, sintered GA-Ni0.1 (Fig. 3(d)) was pore-free and fully densified, but showed rather larger and equiaxed grains. None of the GA-M0.1 powders exhibited abnormal grain growth; even GA-

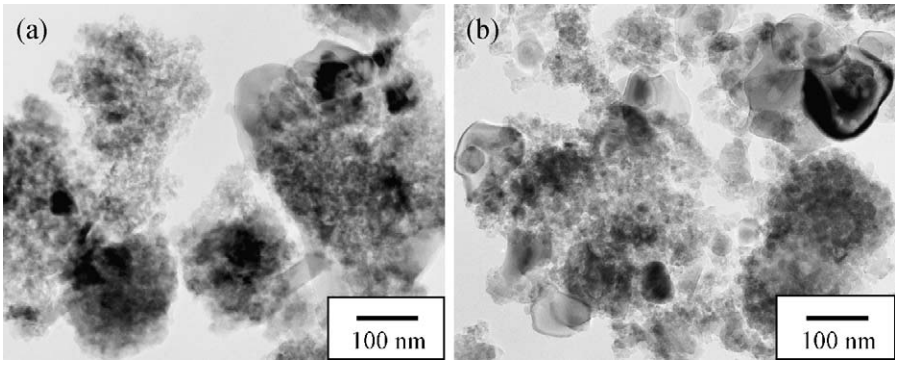

Fig. 2. TEM micrographs of (a) GA-Ca0.1 and (b) GA-Ni0.1 powders.

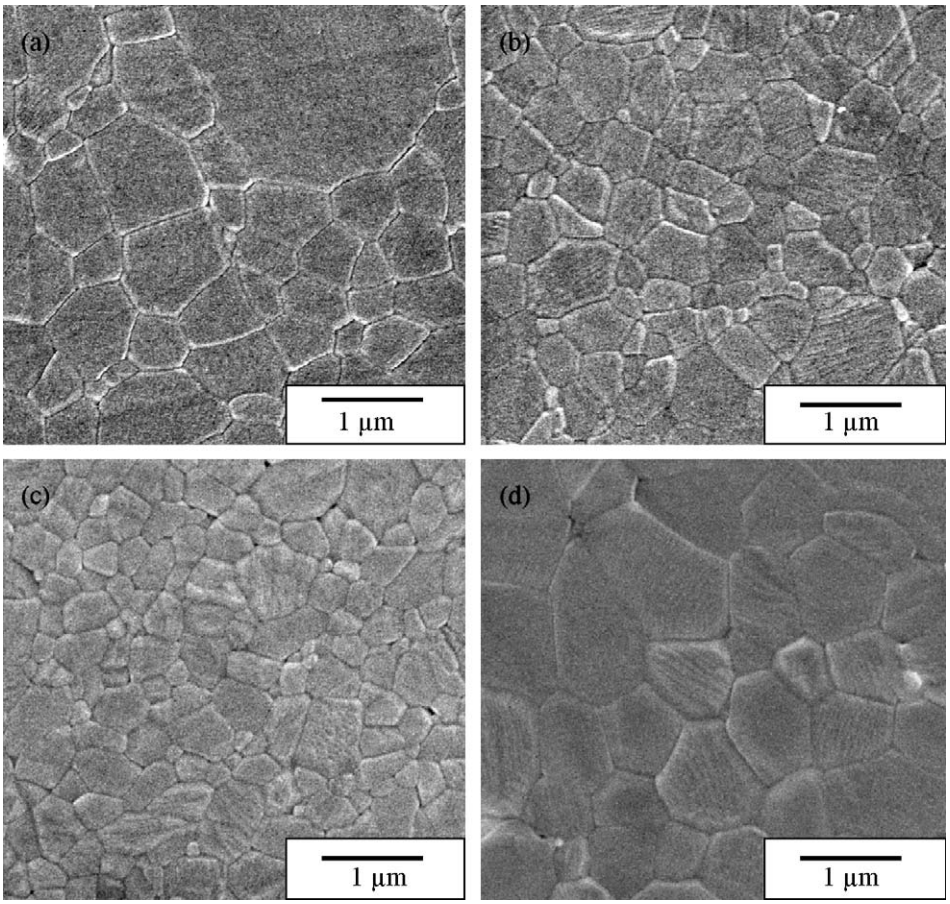

Fig. 3. SEM micrographs of sintered GA-M specimens obtained by PECS at 1250 °C under 80 MPa. (a) GA-M0, (b) GA-Mg0.1, (c) GA-Ca0.1 and (d) GA-Ni0.1.

Ca0.1 could be almost fully densified without triggering abnormal grain growth [23,24].

For a systematic comparison with the data reported previously [21], the average grain size of the sintered GA-Ms obtained by the PECS is plotted against the ionic radius of dopant in Fig. 4, along with that obtained at 1400 °C by pressureless sintering from the same M^{2+}-doped alumina nanopowders. The order of the average grain size in the present PECS study was GA-M0 ≥ GA-Ni0.1 > GA-Mg0.1 > GA-Ca0.1, where the average grain size of GA-M0 was almost the same as that of GA-Ni01, however, the former exhibited a more heterogeneous microstructure, i.e., a wider grain size distribution with larger grains. The order in the average grain size of M^{2+}-doped samples developed by PECS was almost the same as that obtained for M^{2+}-doped γ-alumina powders heated at 1200 °C and 1400 °C in air [21]. This shows that the effect of divalent dopants on grain growth is roughly the same regardless of the sintering method (i.e., PECS vs. pressureless sintering), even though the densification mechanism of PECS differs from that of pressureless sintering because of plastic flow becoming dominant [16].

The densification of fine-grained, polycrystalline alumina is often rate-controlled by grain boundary diffusion [25]. Recently, Yoshida et al. systematically investigated the effect of cation doping (0.1 mol: Mg^{2+}, Mn^{2+}, etc.) on grain boundary diffusivity in alumina ceramics [26]. They showed that the grain boundary diffusivity in alumina is greatly affected by the small amount of dopant cations that segregate to the grain boundary: the improved ionicity in the vicinity of the grain boundary presumably suppresses the atomic diffusion through an increase in the O anion size. Therefore, the change in

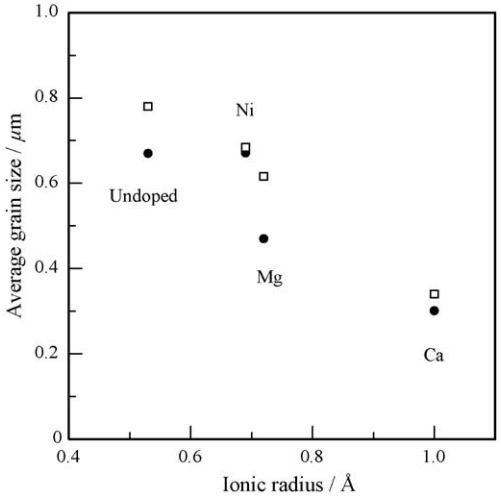

Fig. 4. Average grain size plotted against ionic radius of cation dopant for the sintered GA-M0.1-series specimens obtained by PECS at 1250 °C under 80 MPa (●), along with those obtained by conventional pressureless sintering at 1400 °C (□).

densification and microstructural evolution behaviors of GA-Ms may be ascribed to the change in grain boundary diffusivity even in the PECS process under high pressure: M^{2+} cations expelled from M^{2+}-doped alumina segregate to the grain boundary during transformation/sintering, modulating the grain boundary diffusivity in alumina sintering matrices, and hence affect densification and grain growth. Since the same PECS conditions are employed, the difference in the microstructural evolution behaviors of the GA-M0.1 samples are directly ascribable to the difference in the effects of dopants. These results suggest that the grain boundary diffusivity decreases in the order Ga-Ni0.1 > Ga-Mg0.1 > Ga-Ca0.1, corresponding to the order of increasing ionicity Ga-Ni0.1 < Ga-Mg0.1 < Ga-Ca0.1 in the vicinity of the grain boundary. The nanocrystalline nature of GA-M0.1 powders also seems effective in yielding a submicron-grained microstructure owing to the high dispersion of segregated M^{2+} cations in the sintering matrices. No formation of a secondary phase could be detected by XRD for any of the GA-M0.1 s sintered by PECS. The critical concentration for secondary phase formation depends on the dopant content and the grain size developed. The critical concentration of each M^{2+} dopant without secondary phase formation may relate to the small amount of impurities (SiO_2 and CaO) in the starting powders [13]. Although the mechanism whereby different M^{2+}-dopants have different effects on grain growth inhibition can be explained in terms of the grain boundary diffusivity determined by the dopant species, the present results indicate that except in the case of Ni^{2+}, a M^{2+} dopant content of around 0.10 mass% was sufficient to promote densification with suppressed grain growth through PECS at 1250 °C.

Applying pressure during PECS helps remove pores from the powder compact and provides an additional driving force for low-temperature densification, thus, revealing the advantage of the PECS process, which it shares with hot pressing [27]. It was reported that sintered GA-M0 obtained at 1250 °C under 80 MPa shows a much smaller average grain size (0.67 μm) than that obtained at 1300 °C under 40 MPa (1.75 μm) [16]. This indicates that the high loading pressure of 80 MPa at the lower temperature of 1250 °C employed during the PECS process in this study further leads to a marked decrease in the average grain size. Shen et al. [28] pointed out that the applied pressure provides an extra strain energy, promoting diffusion, however, applying a higher pressure also makes it possible to obtain dense specimens at lower temperatures where grain boundary migration is not yet fully thermally activated. Consequently, under a higher loading of 80 MPa, all GA-M powders could be densified at 1250 °C by further suppressing grain growth. The advantage of the PECS process using GA-M0.1 powders in suppressing grain growth and attaining full densification is obvious because pressureless sintering of GA-Ms powders at 1400 °C resulted in larger average grain sizes in the order GA-M0 (0.78 μm) > GA-Ni0.1 (0.68 μm) > GA-Mg0.1 (0.62 μm) > GA-Ca0.1 (0.34 μm), although pressureless sintering of all GA-M powders did not lead to full densification, yielding a relative density of <95%.

PECS densification of Mg^{2+} (0.1 mass%)-doped α-alumina powders obtained by the impregnation method was reported to be also effective in suppressing grain growth as in the case of conventional sintering techniques, showing that the average grain size of non-doped and Mg-doped samples sintered at 1250 °C under 50 MPa was 1.0 μm (for a normalized comparison, the reported size is divided by 1.56 [29]) and 0.58 μm, respectively [28]. It was also shown that the sintering behavior and densification rate are strongly dependent on the reactivity of the starting powder on the basis of the results of some 20 PECS-treated different commercially available alumina powders: powders having larger specific surface areas sinter and yield homogenous microstructures more easily than do coarse-grained starting powders [28]. However, PECS studies on different cation doped α-alumina powders have been lacking. In this context, the GA-Ca0.1 nanopowder, which exhibits the synergic effect of the Ca dopant and the nanosized nature of the starting powders, is concluded to be the most suitable candidate for tailoring nanocrystalline alumina ceramics, if PECS conditions are further optimized, because the grain size in PECS compacts is strongly dependent on the choice of sintering temperature, pressure, holding time and heating rate [28,30].

4. Conclusions

M^{2+}(M: Mg, Ca, Ni)-doped alumina nanopowders (GA-Ms) were prepared by a new sol–gel route using high-purity polyhydroxoaluminum (PHA) and MCl_2 solutions and then densified by pulse electric current sintering at 1250 °C under a uniaxial pressure of 80 MPa. GA-M0.1 s consisted of a γ-alumina solid solution having M^{2+} cations in the crystal lattice and α-alumina. Ball milling and re-calcination at 900 °C prior to PECS to increase the seeding α-alumina fraction was the key to promoting low-temperature densification. Dense sintered specimens with a uniform microstructure composed of fine and equiaxed grains were obtained from all GA-M0.1 s by PECS at 1250 °C under 80 MPa. Densification and microstructural development strongly depend on the M^{2+} dopant species of the starting nanopowders, and higher loading pressure in the PECS process leads to full densification at lower temperatures, resulting in a more uniform, finer microstructure. M^{2+} cations expelled from M^{2+}-doped alumina nanopowders segregate to the grain boundary during transformation/sintering, modulating the grain boundary diffusivity in the alumina matrices, and hence retard grain growth. The effect of suppressing grain growth depends on the dopant species in the order Ni-doped > Mg-doped > Ca-doped samples. This seems to correspond to the order of M^{2+} segregated grain boundary diffusivity, i.e., correlating with the order of the dopant ionicity in the vicinity of the grain boundary. Fully densified alumina ceramics composed of the finest grains with an average size of 0.30 μm were obtained from GA-Ca0.1 without abnormal grain growth, showing that GA-Ca0.1 has the greatest potential for use in tailoring nanocrystalline alumina ceramics.

Acknowledgements

The authors wish to thank Dr. Yoichi Yajima and Dr. Takayuki Fujita for conducting part of the experiments.

References

[1] A. Krell, A new look at grain size and load effects in the hardness of ceramics, Mater. Sci. Eng. A 245 (1998) 277–284.
[2] D.D. Jayaseelan, S. Ueno, T. Ohji, S. Kanzaki, Differential sintering by improper selection of sintering parameters during pulse electric current sintering, J. Am. Ceram. Soc. 87 (2004) 159–161.
[3] H. Liu, M.E. Fine, Modeling of grain-size-dependent microstructure-controlled sliding wear in polycrystalline alumina, J. Am. Ceram. Soc. 76 (1993) 2393–2396.
[4] A. Krell, P. Blank, H. Ma, T. Hutzler, M.P.B. van Bruggen, R. Apetz, Transparent sintered corundum with high hardness and strength, J. Am. Ceram. Soc. 86 (2003) 12–18.
[5] R.S. Mishra, C.E. Lesher, A.K. Mukherjee, High-pressure sintering of nanocrystalline γ-Al_2O_3, J. Am. Ceram. Soc. 79 (1996) 2989–2992.
[6] O.-H. Kwon, C.S. Nordahl, G.L. Messing, Submicrometer transparent alumina by sinter forging seeded γ-Al_2O_3 powders, J. Am. Ceram. Soc. 78 (1995) 491–494.
[7] Y. Yajima, M. Hida, S. Taruta, K. Kitajima, Pulse electric current sintering and strength of sintered alumina using transition alumina powders prepared from polyhydroxoaluminum gel, J. Ceram. Soc. Jpn. 111 (2003) 110–116.
[8] Y. Yajima, M. Hida, S. Taruta, K. Kitajima, Pulse electric current sintering and strength of sintered alumina using γ-alumina powders prepared by the sol–gel method, J. Ceram. Soc. Jpn. 111 (2003) 419–425.
[9] Y. Yajima, T. Yamaguchi, S. Taruta, K. Kitajima, Effect of milling media purity on pulse electric current sintering and strength of alumina ceramics prepared from transition alumina powder, J. Ceram. Soc. Jpn. 111 (2003) 786–789.
[10] R.L. Coble, Sintering crystalline solids. II. Experimental test of diffusion models in powder compacts, J. Appl. Phys. 32 (1961) 793–799.
[11] P.J. Jorgensen, J.H. Westbrook, Role of solute segregation at grain boundaries during final-stage sintering of alumina, J. Am. Ceram. Soc. 47 (1964) 332–338.
[12] C.A. Handwerker, P.A. Morris, R.L. Coble, Effects of chemical inhomogeneities on grain growth and microstructure in Al_2O_3, J. Am. Ceram. Soc. 72 (1989) 130–136.
[13] S.I. Bae, S. Baik, Critical concentration of MgO for the prevention of abnormal grain growth in alumina, J. Am. Ceram. Soc. 77 (1994) 2499–2504.
[14] H. Song, R.L. Coble, Origin and growth kinetics of platelike abnormal grains in liquid-phase-sintered alumina, J. Am. Ceram. Soc. 73 (1990) 2077–2085.
[15] T. Koyama, A. Nishiyama, K. Niihara, Effect of a small amount of liquid-forming additives on the microstructure of Al_2O_3 ceramics, J. Mater. Sci. 28 (1993) 5953–5956.
[16] M. Hida, Y. Yajima, T. Yamaguchi, S. Taruta, K. Kitajima, Fabrication of submicron alumina ceramics by pulse electric current sintering using Mg^{2+}-doped transition alumina powders, J. Ceram. Soc. Jpn. 114 (2006) 184–188.
[17] T. Fujita, K. Kitajima, S. Taruta, N. Takusagawa, Chemical species in polyaluminum hydroxide solution, Nippon Kagaku Kaishi (1993) 319–328.
[18] A. Odaka, T. Yamaguchi, T. Fujita, S. Taruta, K. Kitajima, Densification of Ca-doped alumina nano-powders prepared from a new sol–gel route with seeding, J. Eur. Ceram. Soc. 28 (2008) 2479–2485.
[19] D. Zhang, L. Zhang, J. Guo, W.-H. Tuan, Direct evidence of temperature variation within ceramic powder compact during pulse electric current sintering, J. Am. Ceram. Soc. 89 (2006) 680–683.
[20] T. Fujita, T. Yamaguchi, N. Takusagawa, K. Kitajima, Formation of activated alumina from polyhydroxoaluminum gels having different [OH/Al] ratios, J. Ceram. Soc. Jpn. 106 (1998) 1017–1022.
[21] A. Odaka, T. Yamaguchi, T. Fujita, S. Taruta, K. Kitajima, Cation dopant effect on phase transformation and microstructural evolution in M^{2+}-substituted γ-alumina powders, J. Mater. Sci. 43 (2008) 2713–2720.
[22] M. Kumagai, G.L. Messing, Controlled transformation and sintering of a boehmite sol–gel by α-alumina seeding, J. Am. Ceram. Soc. 68 (1985) 500–505.
[23] C.W. Park, D.Y. Yoon, Effects of SiO_2, CaO_2, and MgO additions on the grain growth of alumina, J. Am. Ceram. Soc. 83 (2000) 2605–2609.
[24] J.H. Ahn, J.-H. Lee, S.-H. Hong, N.-M. Hwang, D.-Y. Kim, Effect of the liquid-forming additive content on the kinetics of abnormal grain growth in alumina, J. Am. Ceram. Soc. 86 (2003) 1421–1423.
[25] J. Wang, R. Raj, Estimate of the activation energies for boundary diffusion from rate-controlled sintering of pure alumina, and alumina doped with zirconia or titania, J. Am. Ceram. Soc. 73 (1990) 1172–1175.
[26] H. Yoshida, S. Hashimoto, T. Yamamoto, Dopant effect on grain boundary diffusivity in polycrystalline alumina, Acta Mater. 53 (2005) 433–440.
[27] W.D. Kingery, H.K. Bowen, D.R. Uhlmann, Introduction to Ceramics, 2nd ed., John Wiley and Sons, New York, 1976, pp. 501–503.
[28] Z. Shen, M. Johnsson, Z. Zhao, M. Nygren, Spark plasma sintering of alumina, J. Am. Ceram. Soc. 85 (2002) 1921–1927.
[29] M.I. Mendelson, Average grain size in polycrystalline ceramics, J. Am. Ceram. Soc. 52 (1969) 443–446.
[30] Y. Zhou, K. Hirao, Y. Yamauchi, S. Kanzaki, Densification and grain growth in pulse electric current sintering of alumina, J. Eur. Ceram. Soc. 24 (2004) 3465–3470.